12-2024

Capitella teleta gets left out: possible evolutionary shift causes loss of left tissues rather than increased neural tissue from dominant-negative BMPR1

Nicole B. Webster

Néva P. Meyer

Neural Development

RESEARCH

Open Access

Capitella teleta gets left out: possible evolutionary shift causes loss of left tissues rather than increased neural tissue from dominant-negative BMPR1

Nicole B. Webster[1,2] and Néva P. Meyer[1*]

Abstract

Background The evolution of central nervous systems (CNSs) is a fascinating and complex topic; further work is needed to understand the genetic and developmental homology between organisms with a CNS. Research into a limited number of species suggests that CNSs may be homologous across Bilateria. This hypothesis is based in part on similar functions of BMP signaling in establishing fates along the dorsal-ventral (D-V) axis, including limiting neural specification to one ectodermal region. From an evolutionary-developmental perspective, the best way to understand a system is to explore it in a wide range of organisms to create a full picture.

Methods Here, we expand our understanding of BMP signaling in Spiralia, the third major clade of bilaterians, by examining phenotypes after expression of a dominant-negative BMP Receptor 1 and after knock-down of the putative BMP antagonist Chordin-like using CRISPR/Cas9 gene editing in the annelid *Capitella teleta* (Pleistoannelida).

Results Ectopic expression of the dominant-negative Ct-BMPR1 did not increase CNS tissue or alter overall D-V axis formation in the trunk. Instead, we observed a unique asymmetrical phenotype: a distinct loss of left tissues, including the left eye, brain, foregut, and trunk mesoderm. Adding ectopic BMP4 early during cleavage stages reversed the dominant-negative Ct-BMPR1 phenotype, leading to a similar loss or reduction of right tissues instead. Surprisingly, a similar asymmetrical loss of left tissues was evident from CRISPR knock-down of *Ct-Chordin-like* but concentrated in the trunk rather than the episphere.

Conclusions Our data highlight a novel asymmetrical phenotype, giving us further insight into the complicated story of BMP's developmental role. We further solidify the hypothesis that the function of BMP signaling during the establishment of the D-V axis and CNS is fundamentally different in at least Pleistoannelida, possibly in Spiralia, and is not required for nervous system delimitation in this group.

Keywords Bone morphogenetic protein, Dominant negative, CRISPR, Annelida, *Capitella*, Evo-devo, Neural development

*Correspondence:
Néva P. Meyer
nmeyer@clarku.edu
Full list of author information is available at the end of the article

Background

The nervous system is an important animal innovation whose origins are poorly understood, especially the evolution of central nervous systems (CNSs). Many questions remain about the evolutionary and developmental processes that have allowed for the great diversity of extant nervous systems. Only after we have a full picture of nervous system diversity and how nervous systems develop can we start to answer big evolutionary questions: Have CNSs evolved repeatedly? What parts of CNSs may be homologous? What can that tell us about the evolution of complex systems in general? Are gene networks repeatedly co-opted to form analogous systems?

In many bilaterian animals with a CNS, neural tissue is localized along the dorsal-ventral (D-V) axis, e.g., vertebrates have a dorsal neural tube, whereas arthropods and annelids have a ventral nerve cord. A key part of the D-V axis and CNS formation in some vertebrates and ecdysozoans are the Bone Morphogenetic proteins (BMPs), which belong to the Transforming Growth Factor β (TGF-β) superfamily. In these groups, a gradient of BMP signaling helps establish fates along the D-V axis, including limiting where neuroectoderm forms [1]. Later in development, a BMP gradient patterns neural subtypes along the D-V axis of the CNS itself [2]. As with other members of the TGF-β superfamily, BMPs are secreted ligands that dimerize and bind to a tetrameric, extracellular receptor complex made up of two type I and two type II receptors [3]. The type II receptor phosphorylates the type I receptor once the ligand is bound, causing the type I receptor to phosphorylate a transcription factor, Suppressor of Mothers against Decapentaplegic (SMAD), which then binds a co-SMAD and moves into the nucleus to affect gene transcription. Secreted BMP inhibitors such as Chordin/Short gastrulation (Chd/Sog) are proposed to be the key regulators of the BMP signaling gradient [4]. Thus, BMP's anti-neural function is intrinsically linked to its organizing function in D-V axis formation [2].

One prevailing hypothesis suggests that a CNS evolved once, near the base of Bilateria, such that the brains and nerve cords of all bilaterians are homologous [5–7]. This hypothesis is intertwined with the idea of axis inversion, where the CNS and D-V axis became inverted in the last common ancestor of chordates, which could explain why BMP signaling is anti-neural in both groups, forming a dorsal nerve cord in vertebrates and a ventral nerve cord in insects. Recent work has contested this hypothesis, at least partially because the function of BMP signaling during D-V axis and CNS formation differs between some spiralians and the rest of Bilateria [8–12]. Additionally, work outside traditional lab species in other lineages shows that within both deuterostomes (Enteropneusta [13]) and ecdysozoans (Nematoda, Onychophora [14]), the role of BMP signaling in D-V axis and neural specification is more complicated than generally described.

Within spiralians, the role of BMP signaling during CNS fate specification and D-V axis formation has been difficult to pinpoint [11, 15]. For example, in the mollusc *Ilyanassa* (~*Tritia*) *obsoleta* (Say, 1822) [16], BMP signaling appears to play a role in D-V organization, where a loss of BMP signaling caused a loss of the D-V axis but did not repress neural tissue formation [17]. Instead, ectopic BMP caused ectopic eye and brain formation. In contrast, in the mollusc *Crepidula fornicata L.*, ectopic BMP caused a partial loss of the head (episphere) but a normal trunk [15]. A more complex study in *Lottia peitaihoensis (was named L. goshimai)* (Grabau & S. G. King, 1928) showed that perturbations of BMP or Chd/Sog affected both eye number and D-V axis organization, but how CNS tissue was affected is unclear [18]. In the annelid *Platynereis dumerilii* (Audouin & Milne Edwards, 1833), ectopic BMP shifted the D-V boundaries of gene expression in the neuroectoderm, but did not shift neuroectodermal boundaries as assayed by expression of the pan-neuronal gene *Pdu-elav* [7]. In the leech *Helobdella*, gain and loss of BMP signaling affected the D-V identity of the 'o' and 'p' ectodermal bandlets in the trunk but not in the rostral segments; no effect was reported for the neural (n) bandlet [19, 20]. In the annelid *Capitella teleta* Blake, Grassle & Eckelbarger, 2009 [21], we previously showed that ectopic BMP does not reduce neural tissue or affect D-V axis formation [11]. Instead of BMP, Activin/Nodal organizes the D-V axis in *C. teleta* [8, 9, 22, 23]. Some spiralians do show a predicted response to disruption of BMP signaling. In brachiopods, drug-induced knockdown of BMP signaling caused ventralization and increased the expression of neural markers [24]. In planarians, BMP disruption via RNAi created a duplicate dorsal nervous system [25]. Overall, these diverse results raise questions about the ancestral function of BMP signaling during D-V axis and CNS formation in Spiralia.

The lack of consensus on how BMP signaling functions in spiralians is at least partially due to a lack of functional studies and to differences in methodology across studies. In *C. teleta,* there are two BMP ligands, Ct-BMP2/4 and Ct-BMP5–8, and two BMP receptors, a type 1, Ct-BMP Receptor 1 (BMPR1 = Alk3/6 Activin receptor-like kinase) and a type 2, Ct-BMP Receptor 2 (BMPR2) [26]. Based on models of BMP signaling in vertebrates and insects, both ligands are thought to signal to the nucleus using the phosphorylated receptor-regulated SMAD, SMAD1/5/8, and a co-SMAD, SMAD4, although ActivinR1 (ALK1/2) may also bind BMP5–8 and transmit

through the other rSMAD, SMAD2/3 [3]. A key antagonist in the system, Chd/Sog, normally regulates the BMP gradient. While Chd/Sog has been lost in many annelids, Chordin-like (Chd-l) may play a similar role [27].

We previously showed that ectopic BMP does not disrupt overall D-V axis formation or reduce the amount of CNS tissue formed in *C. teleta* embryos [11]. Here, we examine the effect of altering BMP signaling in *C. teleta* using a dominant-negative Ct-BMPR1 and knock-down of *Ct-Chd-l* via CRISPR/Cas9 gene editing. We truncated the kinase domain of BMPR1, creating a dominant-negative BMP receptor (BMPR1ΔK) that decreased downstream phosphorylation of SMAD1/5/8 but did not increase CNS tissue or alter overall D-V axis formation in the trunk. Instead, BMPR1ΔK injection resulted in a unique asymmetrical phenotype: a distinct loss of left tissues including the left eye, brain, foregut, and trunk mesoderm. A similar asymmetrical loss of tissue was evident from CRISPR knock-down of *Ct-Chd-l*. Overall, we show added symmetry-related functions of BMP signaling in spiralians and provide more evidence that BMP signaling has no role in limiting neural specification in this annelid.

Material and methods

Animal care and embryo collection

Adults of *Capitella teleta* were cultured in glass finger bowls with 32–34 ppt artificial seawater (ASW; Instant Ocean Sea Salt in Hydro Picopure-filtered tap water) at 19 °C and fed with sieved mud collected from the local coastline [28–30]. In order to collect embryos of the correct stage (st.), mating dishes were generated by separating males and females for 3–5 days at 19 °C and then either 1) combining males and females for 5–16 h in the dark at 19 °C or 2) exposing males and females for 6+ h to light at room temperature (RT, ~21°C) and then combining them for 5 h at RT [22]. Embryos and larvae, except where otherwise noted, were raised in ASW with 50 µg/mL penicillin and 60 µg/mL streptomycin (ASW+PS) at RT. ASW+PS was changed once or twice daily.

Isolation of *C. teleta BMP receptor 1*

Total RNA was extracted from mixed stage 1–9 embryos and larvae using the RNA Trizol extraction protocol (Molecular Research Center, Inc.) or the RNeasy Mini Kit (Qiagen cat. 74104) paired with the QIAshredder columns (Qiagen 79656). Reverse transcription reactions were conducted using the SMARTer RACE kit (Clontech 634859) or High-capacity cDNA Reverse Transcription kit (Applied Biosciences 4368814). Only one BMP Receptor 1 (*Ct-BMPR1*) homolog has been identified in the *C. teleta* genome [26]. A 1533 bp fragment of *Ct-BMPR1* (JGI PID111904) encoding nearly the entire coding sequence (but lacking the last 54 bp at the end of the 3' UTR) plus 25 bp of 5'-UTR was amplified by PCR using 3 sets of overlapping gene-specific primers (Table 1), followed by a nested PCR using the SMARTer RACE kit following the manufacturer's protocol. The sequence we isolated was confirmed via BLAST [31] with 67% protein sequence identity compared to *Platynereis dumerilii* (CAE76647.1) and 66% with *Lamellibrachia satsuma* [32] (KAI0231297.1). The retained domains include the BMP binding domain, transmembrane domain, and GS domain.

BMPR1ΔK construction

Ct-BMPR1 domains were determined by aligning protein sequences with previously published BMPR1 sequences (*Drosophila melanogaster*, AAA61947.1, *Xenopus laevis*, BAA22438.1, *Platynereis dumerilii* CAE76647.1, *Helobdella sp. Austin* JN091774.1). The dominant-negative BMPR1ΔK was designed by truncating *Ct-BMPR1* at amino acid (aa) 221 to remove the kinase domain, following previously-designed dominant-negative BMPR1 constructs [20, 33, 34]; see Supplemental Fig. 1. The designed dominant-negative sequence (aa 1–220) was synthesized (Eurofins) for use in the Gateway system (Invitrogen) and ligated into an entry vector using the pENTR/D-TOPO Cloning Kit with One Shot™ TOP10 Chemically Competent *E. coli* (Invitrogen K2400-20). Following Gateway manufacturing protocols, we constructed a fusion protein with Ct-BMPR1ΔK and mVenus using pSPE3-RfA-Venus [35] and LR Clonase II (Invitrogen 11791-020), and the final expression vector, pSPE3 *Ct-BMPR1ΔK::mVenus*, was verified by sequencing. mRNA was then transcribed using the mMESSAGE mMACHINE™ T3 Transcription kit (Invitrogen AM1348), a polyA tail was added with the Poly(A) Tailing kit (Invitrogen AM1350), and mRNA was purified with the MEGAclear kit (Invitrogen AM1908) and concentrated with an ammonium acetate precipitation. mRNA was resuspended in RNAse-free water (Invitrogen AM1908), and a Nanodrop One

Table 1 Ct-BMPR1 specific primers

Forward	Reverse
5'-GCTGTGTTTTTGTTGCTCGG	5'-CTGAGAGCGATCGATTAATTCCT
5'-GGCATCGAATGCTACTGCAA	5'-CCACGATCCCGTACCTTTGA
5'-AGCAGCTGACATCAAAGGTACG	5'-GCGTTATTTTCGGCATTTTCCA
5'-RACE	5'-CAGAGGAGGGCTCCCTCATGCAGT
5'-RACE nested	5'-AGAACTCAGGACGTTTGGCTG TCTGCCT

(Thermo Scientific) was used to determine concentration. *BMPR1ΔK::mVenus* mRNA was then aliquoted for single-use and stored at -80 °C following Layden et al. [36] and Özpolat et al. [37].

CRIPSR/Cas9

CRISPR knock-downs were designed and verified following Neal et al. [38]. Two 20 bp sgRNA target sequences (sgRNA175: AGTGCCGCAAGACTCTTG TG; sgRNA264: CCACGGGAGTCGTGTATCCA) and amplification primers were designed using CRISPOR [39] for NGG PAM sequences near the 5' end of *Ct-chd-l* (JGI PID224618) [26, 40] with minimal off target complementarity with the *C. teleta* genome. Complete sgDNA templates were assembled and amplified using the T7 promoter (Phusion High Fidelity, NEB E0553). sgRNA was then transcribed (MEGAshortscript T7, Invitrogen AM1354), cleaned (RNA Clean and Concentrator, Zymo Research R1013) and aliquoted to 1 µg/µL in RNAse-free water at -80 °C for storage (concentration was determined using a Qubit 3 Fluorometer, Invitrogen).

Verification of *in vitro* cutting was confirmed by adding 250 ng of each sgRNA and 500 ng of Cas9 protein (PNA Bio cat. CP01-200) to 250 ng of PCR-amplified *Ct-chd-l* and incubating at RT for 1 h. The sample was then run on a 1% agarose gel. The expected cut site was amplified via PCR using *Ct-chd-l* specific primers (175L: CGAGAG GACGACAACCAGAG; 175R: TTGTGCGTTTCCTGC GAAAG). Verification of i*n vivo* Cas9 cutting of *chd-l* following Neal et al. [38]. Briefly, the genomes of individual stage 6 larvae were extracted after Cas9/sgRNA injection as zygotes and sent for sequencing using *Ct-chd-l* specific primers. Four of nine larvae that were sequenced showed evidence of cleavage and subsequent mutations via CRISPR although cleavage of both *Ct-chd-l* copies could not be verified. Repeated sequencing failure was assumed to indicate more severe mutations in three specimens.

Microinjection

Prior to injection, the outer egg envelope of zygotes or early cleavage-stage embryos was permeabilized for 30 sec using a freshly mixed, 1:1 solution of 1 M sucrose and 0.25 M sodium citrate (individual solutions were prepared the previous day, stored at 4°C and then warmed to RT before use). Egg envelope permeabilization was followed by three rinses with ASW+PS. DiI (1,1'-dioctadecyl-3,3,3'3'-tetramethylindocarbocyanine perchlorate) injections into cleavage-stage embryos were conducted following Meyer et al. [41] for lineage tracing. mRNA and sgRNAs/Cas9 were injected into zygotes. In *C. teleta*, the time to first cleavage after fertilization has not been carefully determined but appears to be ~4–6 h at 19°C. Because fertilizations are likely internal in *C. teleta* [42], the precise timing of fertilization for the collected zygotes was unknown. In general, zygotes started cleaving to two cells anywhere from a few minutes to a few hours after injection. mRNA injections were performed with beveled (Sutter BV-10) Quartz needles (Sutter Instrument Co., Novata, CA, USA), where needles were pre-warmed to 55 °C before being backfilled to decrease the time needed to backfill the needles. The injectant was mixed with 5x Rhodamine-Dextran (30 mg/mL Dextran Tetramethylrhodamine 10k MW Invitrogen D1868) as a tracer and a 5x injection buffer (10 mM HEPES pH 7.0; 75 mM KCl) [43] in RNAse-free water to a final concentration of 1x for both. BMPR1ΔK mRNA concentrations ranging from 480 ng/µL to 1.6 µg/µL were injected with no changes in resulting phenotypes. For *Ct-chd-l* CRISPR, needles were backfilled with 125 ng/µL of each sgRNA and 2 µg/µL Cas9 protein, rested for 10 min at RT, then stored at 4 °C for up to 5 days. Some animals were mounted in ASW+PS for live imaging of mVenus expression (AxioImager M2 microscope (Zeiss); coverslips were sealed with vacuum grease to reduce evaporation. Both injected animals and uninjected controls from the same brood were raised at RT in ASW+PS until stage 6, and then animals were fixed and labeled for phenotypic scoring. An experiment was not scored unless 90% of the uninjected animals were healthy.

Incubation in BMP protein

To understand the interaction between BMPR1ΔK and BMP protein, BMPR1ΔK-injected animals (2 different broods as 2 biological replicates) and uninjected control animals were incubated in 250 ng/mL BMP4 protein in ASW+PS for 12 h starting at either at the 8-cell stage (first-quartet of micromeres or "1q") or just after birth of micromere 4d (~64-cell stage or "4q"). Stock recombinant zebrafish BMP4 protein (R&D Systems 1128-BM-010) was reconstituted to 20 µg/mL in 0.1% bovine serum albumin (BSA) and 4 mM HCl in Picopure water, aliquoted and stored at -80°C [11]. Animals were raised until stage 6 in ASW+PS and then fixed to assess the resulting phenotypes.

Whole mount in situ hybridization

Whole mount in situ hybridization (WMISH) was conducted as described previously [44]. Briefly, all WMISH fixations were done in 4% paraformaldehyde (PFA, stock 32% PFA ampules from Electron Microscopy Sciences, cat. 15714) in ASW for 6 h–overnight at 4 °C. After fixation, animals were serially dehydrated in methanol and stored at -20 °C. Animals were hybridized for a minimum of 72 h at 65 °C with 1 ng/µl of each probe. Spatiotemporal RNA localization was observed using an NBT/BCIP

color reaction. The color reaction was stopped using 3 washes of PBS with 0.1% Tween-20. After WMISH, animals were labeled with Hoechst and anti-acetylated-Tubulin (details below), cleared in 80% glycerol in PBS, and mounted on slides for DIC and fluorescent imaging.

Fixation, staining, and antibody labeling in larvae

Prior to fixation, the egg envelope of embryos was permeabilized for 3 min using a freshly mixed 1:1 solution of 1 M sucrose and 0.25 M sodium citrate. In the case of larvae, they were relaxed in 1:1 ASW:0.37 M $MgCl_2$ for 5–10 min before fixation. Immunolabeling was carried out as in Meyer et al. (2015). Animals were fixed for 30 min with 4% PFA in ASW at RT, rinsed with PBT (PBS + 0.1% Triton-X 100), blocked in 5 or 10% heat-inactivated goat serum in PBT (block) and incubated in primary antibody in block overnight at 4 °C. Secondary antibodies in block were incubated overnight at 4 °C, then animals were thoroughly washed with PBT, cleared, and mounted in SlowFade Gold (Life Technologies, cat. S36936) for confocal laser scanning microscopy or in 80% glycerol in PBS for all other types of microscopy. All washes and exchanges were done in RainX-coated (RainX) glass spot dishes. Primary antibodies used were as follows: 1:800 rabbit anti-serotonin (5HT; Sigma-Aldrich, cat. S5545), 1:20 mouse anti-Futsch (clone 22C10, Developmental Studies Hybridoma Bank), 1:800 mouse anti-acetylated-Tubulin (ac-Tub; clone 6-11B-1, Sigma, cat. T6793), and 1:400 rabbit anti-phosphorylated-SMAD1/5/8 (pSMAD1/5/8; clone 41D10, Cell Signaling Technologies). Secondary antibodies used were as follows: 1:2000 goat anti-mouse F(ab')2 Alexa488 (Sigma-Aldrich, cat. F8521) and 1:1000 sheep anti-rabbit F(ab')2 Cy3 (Sigma-Aldrich, cat. C2306). F-actin and DNA staining were performed by incubating the embryos and larvae in 1:100 BODIPY FL-Phallacidin (Life Technologies, cat. B607; stock concentration 200 Units/mL in methanol), 0.1 µg/mL Hoechst 33342 (Sigma-Aldrich, cat. B2261) along with the secondary antibodies.

pSMAD immunolabeling in cleavage-stage embryos

To detect levels of BMP signaling after injection, the amount of phosphorylated-SMAD1/5/8 in the nucleus was measured (2 biological replicates). Embryos were separated into four treatments: Uninjected embryos incubated for 1 h in (1) ASW or (2) BMP; BMPR1ΔK-injected embryos incubated for 1 h in (3) ASW or (4) BMP; 250 ng/mL recombinant BMP4 was added at the 4q stage (~8–10h after injection) as previously described [11]. Then the embryos were fixed for 15 min in 4% PFA at RT, and all other steps were carried out as above. Animals were labeled with 1:400 anti-phosphorylated-SMAD1/5/8 (clone 41D10, Cell Signaling Technologies), BODIPY FL-Phallacidin, and Hoechst 33342 as above.

All animals went through immunolabeling at the same time using the same protocol, and images were all taken on the same microscope (Confocal TCS SP5-X, Leica) using the same settings to control for differences in fluorescence. pSMAD1/5/8 levels were determined by averaging the fluorescence brightness of the anti-pSMAD1/5/8 antibody in the nucleus of the surface-most cells that were intact (not dividing) and did not appear distorted by the edge of the embryo. These 3–5 nuclei per animal were each measured 3 times with a newly drawn ROI on different days to reduce measurement bias and averaged in Leica Applications Suite X (Leica). Since embryos were imaged from different orientations, different cells were measured for each embryo.

Microscopy and figure preparation

Images were taken using DIC optics on an AxioImager M2 microscope (Zeiss) with an 18.0-megapixel EOS Rebel T2i digital camera (Canon) for WMISH animals or an AxioCam MRm rev.3 camera (Zeiss) with Zen Blue software (Zeiss) for antibody-labeled animals or live imaging of mVenus. DiI-labeled animals were imaged using a Zeiss Apotome.2 to produce optical sections. Animals for confocal laser scanning microscopy were imaged using a TCS SP5- X (Leica). DIC images taken at different focal planes were merged with Helicon focus 7 (Helicon). Different channels and z-stacks of fluorescent images were merged using Zen Blue (Zeiss). WHISH images were edited for contrast and brightness using Adobe Photoshop CC (Adobe). Figure panels were assembled with Adobe Illustrator CC (Adobe).

Statistics and analyses

Only elongated animals, i.e., an ellipsoid body shape with all of the following: brain, ventral nerve cord (VNC), prototroch and telotroch, were scored for phenotypes (see Results for details). All statistics were performed in R/RStudio 1.2.5 (R Core team, 2014; RStudio Team, 2012), and all graphs were created using the ggplot2 package (Wickham, 2009) and polished with Adobe Illustrator CC (Adobe). Model testing was used determine the appropriate covariables to analyze in each ANOVA; the R package rcompanion (Mangiafico., 2015) was used, and the model with the lowest AIC (Akaike information criterion) was chosen. Tukey post-hoc analyses were used to determine the differences between treatments.

Results

BMPR1ΔK-injected animals expressed mVenus

To determine if BMPR1ΔK was expressed in embryos, we looked for the expression of the mVenus tag after injection using live imaging. mVenus fluorescence was first observable during early cleavage, 4–7 h after *BMPR1ΔK::mVenus* mRNA was injected into zygotes (n = 3 broods; 1 brood = 1 biological replicate), Fig. 1 shows mVenus 20 h after injection), and fluorescence was generally not detectable by 36 h (n = 8 broods). However, mVenus fluorescence lasted much longer in two broods, until st. 5, where larvae are just beginning to move by ciliary beating (~4 days post injection). mVenus fluorescence was detectable in most cells in cleavage-stage embryos and was localized to cellular membranes, with additional punctate fluorescence surrounding the nucleus. This suggests a low degree of mosaicism and that the truncated receptor protein was properly localized to the membrane. While the intensity of mVenus fluorescence varied between broods and individuals, injected animals showed similar phenotypes, even in animals with no observable mVenus fluorescence. This suggests that BMPR1ΔK protein is produced across a range of mRNA concentrations and is able to function similarly, even in embryos where mVenus fluorescence is not detectable.

BMPR1ΔK can reduce nuclear pSMAD1/5/8

To determine if BMPR1ΔK affected downstream signaling of the BMP pathway, we assayed pSMAD1/5/8 activation in embryos after injection. We previously showed that ectopic BMP4 increased pSMAD1/5/8 activation in *C. teleta* [11], and this was used as a positive control. Uninjected controls and BMPR1ΔK-injected embryos (with or without ectopic BMP4) generally had low to non-detectable amounts of nuclear pSMAD1/5/8, whereas uninjected embryos with ectopic BMP4 showed a significantly higher level of nuclear pSMAD1/5/8 than either uninjected controls or BMPR1ΔK-injected embryos (ANOVA, $F_{treatment} = 150.75$, df = 3, $p < 0.0001$; Tukey HSD $p < 0.0001$; Fig. 2). In some uninjected controls, nuclear pSMAD1/5/8 levels varied between non-dividing cells; some nuclei appeared to have higher levels of pSMAD1/5/8 compared to their neighbors (cyan versus white arrows in Fig. 2). Interestingly, the BMPR1ΔK-injected embryos did not appear to have the same variation in nuclear pSMAD1/5/8 levels within an embryo, with or without added BMP4. In summary, BMPR1ΔK injection was able to block an increase in nuclear pSMAD1/5/8 when ectopic BMP4 was added, suggesting that BMPR1ΔK protein is able to block activation of the BMP pathway in *C. teleta*.

BMPR1ΔK injection produced left-reduced, asymmetrical features

The majority (55.6% ± 5.3 SE) of BMPR1ΔK-injected zygotes (n = 420, 13 broods) did not elongate. Un-elongated embryos presented a broad range of features but were generally more spherical than controls, and none had all of the following: brain, ventral nerve cord (VNC), prototroch, telotroch (Suppl. Fig. 2). There was no significant effect of *BMPR1ΔK::mVenus* mRNA concentration on the proportion of elongated embryos, but injected embryos with added ectopic BMP4 did elongate significantly more often (82.4% ± 0.1 SE; n = 2; T-test, df = 12, t = 3.0, $p < 0.006$). Only elongated animals were further scored for phenotypic changes relating to BMPR1ΔK-injection.

While most elongated BMPR1ΔK-injected animals were relatively normal at st. 6, the most common, non-wild-type phenotype was a general reduction or loss of tissue on the left side. This included the brain lobe and larval eye on the left side of the episphere, and the foregut, mesodermal band and muscle fibers on the left side of the trunk (Figs. 3, 4, 5). This trait asymmetry appears to be correlated; the asymmetry of brain lobes, foregut,

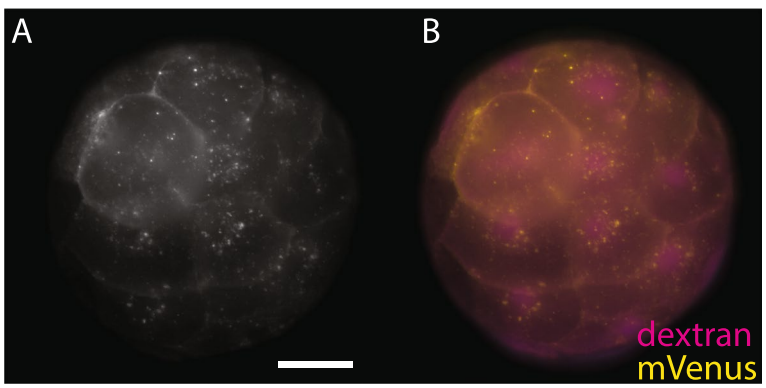

Fig. 1 mVenus expression 20 hour after injection of 1.6 µg/µL mRNA encoding BMPR1ΔK::mVenus into a zygote. **A** mVenus. **B** merged image; mVenus (yellow) and Rhodamine-Dextran (magenta, tracer dye). Scale bar: 50 µm

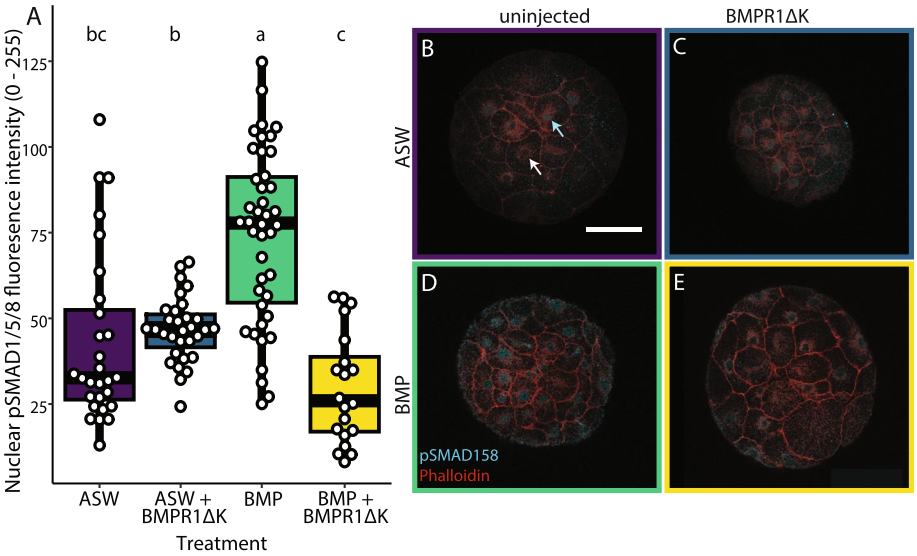

Fig. 2 Nuclear pSMAD1/5/8 levels approximately 10 h after BMPR1ΔK injection. **A** Boxplot showing the varying effect of BMPR1ΔK injection on the amount of nuclear pSMAD1/5/8 (measured as the relative brightness of labeling with an anti-pSMAD1/5/8 antibody in the nucleus); uninjected BMP-treated animals had significantly more nuclear pSMAD1/5/8 than animals without added BMP, while BMPR1ΔK-injected, BMP-treated animals have significantly less nuclear pSMAD1/5/8 than all treatments except seawater controls. Letters (a, b, c) indicate significance groups; white dots indicate individual cells. **B** Uninjected embryo in ASW, Arrows: cyan: higher nuclear pSMAD1/5/8; white: lower/no nuclear pSMAD1/5/8. **C** BMPR1ΔK-injected embryo in ASW. **D** Uninjected embryo with 1 h BMP4 pulse. **E** BMPR1ΔK-injected embryo with 1 h BMP4 pulse. Cyan: pSMAD1/5/8; Magenta: Phalloidin. Scale bar: 50 µm

or mesoderm tissue was not independent (pairwise Fisher's exact tests, $p < 1x10^{-09}$) such that animals lacking a left brain lobe were more likely to also lack their left mesoderm than chance. Furthermore, concentrations of *BMPR1ΔK::mVenus* mRNA ranging from 480 ng/µL to 1.6 µg/µL were injected with no significant changes in the proportion of resulting phenotypes (foregut, brain, and mesoderm asymmetry; $t_{paired}(2) = 2.4$, $p = 0.14$).

Brain

The majority of BMPR1ΔK-injected animals ($n = 130$) showed two wildtype brain lobes (concentrations of nuclei in the brain region; 77%; Figs. 3B, 5), with the second most likely phenotype being animals with only a single brain lobe (21%). There was a strong asymmetry in brain lobes; 22% had a reduced or missing left brain lobe, while only 1% showed a reduced right brain lobe (Figs. 3A–D, 5). Brain asymmetry was also apparent in SC^{ac+} cells (acetylated tubulin$^+$ sensory cells [45]; $n = 48$), which were reduced on the left side 27% of the time, and $5HT^+$ cells ($n = 24$), which were reduced on the left side 12.5% of the time. *Ct-elav1*$^+$ brain tissue ($n = 28$) was usually symmetrical (71%), yet a reduction or loss of the left side was common (25%), and a reduction on the right side was rare (4%) (Figs. 3E–L, 5). The level of *Ct-elav1*$^+$ expression in the episphere was not quantified but was qualitatively slightly lower in BMPR1ΔK-injected animals relative to controls. Notably, the majority of animals lacked $5HT^+$ neurons in the brain (50%) compared to only 1% lacking SC^{ac+} cells. In all cases, asymmetrical reduction of SC^{ac+}, $5HT^+$ or *Ct-elav1*$^+$ cells was associated with asymmetry in the brain lobes. While the degree of asymmetry varied between measures of brain phenotype, the most likely abnormal phenotype was a reduction or loss of the left brain lobe.

Eyes

Approximately 50% of BMPR1ΔK-injected animals ($n = 180$) had one left and one right orange larval eye pigment cell (wild-type phenotype; Figs. 4, 5; Supplemental Table 1), while 32% of injected animals had a reduction in the number of left eye pigment cells and 4% had a reduction in the number of right eye pigment cells. The majority of these were 1-eyed animals (25% right eye pigment cell only, 2% left eye pigment cell only), but some animals did have medial eye pigment cells or multiple left or right eye pigment cells. 9% of BMPR1ΔK-injected animals had no eye pigment cells. While the number and placement of eye pigment cells varied between abnormal phenotypes, a reduction of loss of left eye pigment cells was most common. We also noticed a possible decrease in the number of brown pigment cells (i.e., melanocytes) in the episphere in BMPR1ΔK-injected animals, but this was not quantified.

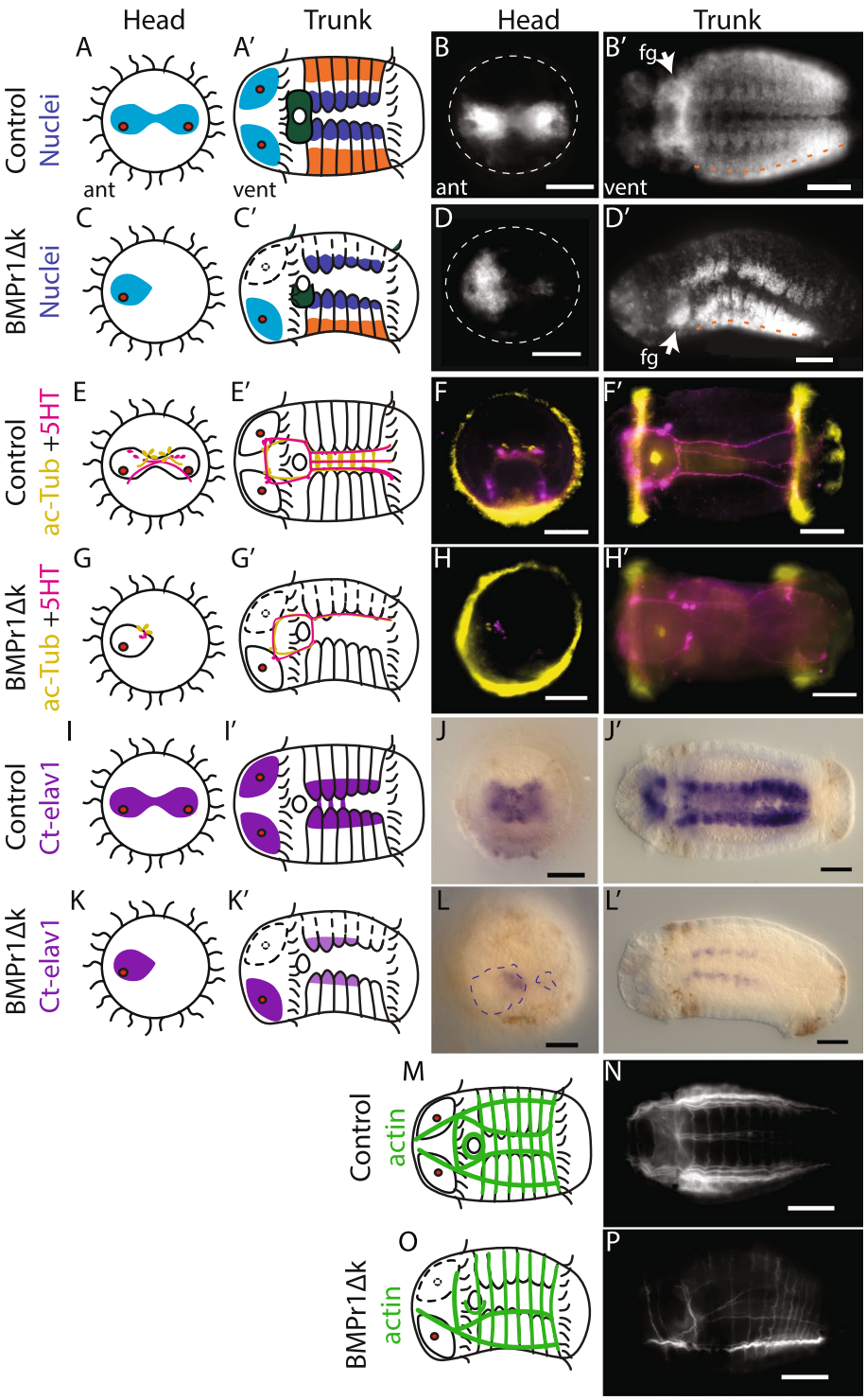

Fig. 3 Diagrams and images of representative control and BMPR1ΔK-injected animals. **A**–**D** Phenotypes visible via nuclear staining (Hoechst): brain lobes (cyan), foregut (dark green), hemiganglia of the ventral nerve cord (blue), and mesodermal bands (orange). White dashed lines: episphere outline; orange dashed line: division between mesoderm and non-neural ectoderm. **E**–**H** Neurons and neurites (ac-Tub: yellow, 5HT: magenta). **I**–**L** Post-mitotic neurons (anti-*Ct-elav1* ISH) Blue dashed lines: brain. **M**–**P** Muscle fibers (Phalloidin). See text for numbers of animals. For **D**, **H** and **L**, the anterior and ventral views are from different animals to illustrate the generalized phenotype. Scale bars: 0.5 µm

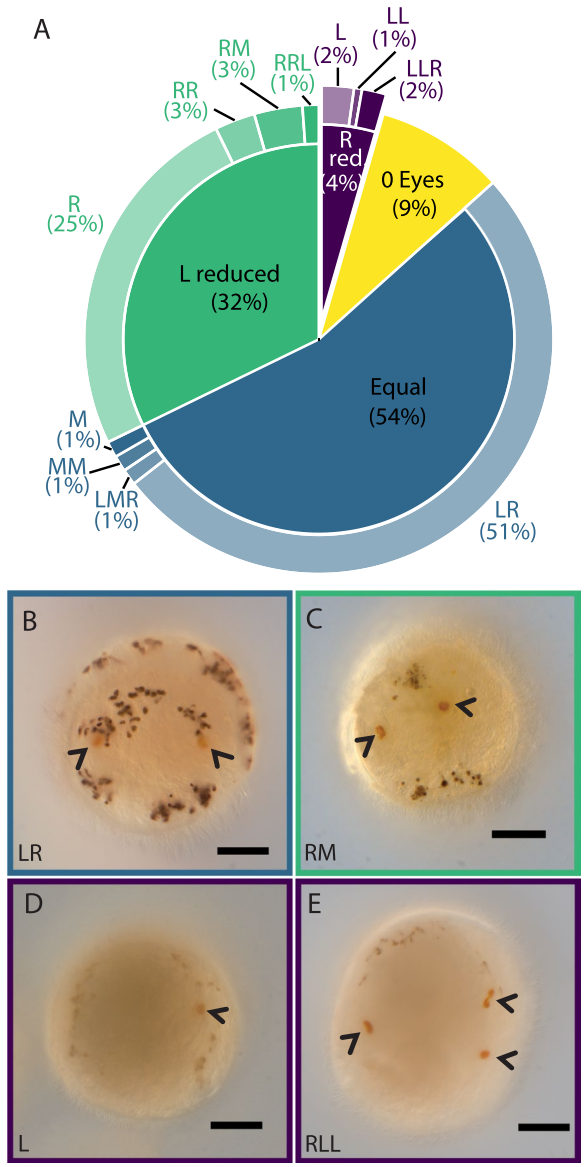

Fig. 4 Eye formation after BMPR1ΔK-injection. **A** Pie chart showing the proportion of each larval eye pigment cell phenotypes: Equal (blue), right-biased (green) and left-biased patterns (purple) were further sub-divided based on the number of eye pigment cells in each position, e.g., RM indicates 1 right and 1 medial eye pigment cell; R, right; L, left; M, medial. **B**–**D** Larval eye pigment cells (orange, arrowheads). **B** Wildtype. **C** Right and middle eye pigment cells. **D** Left eye. **E** One right and two left eye pigment cells. Scale bars: 0.5 µm

Foregut

Foregut tissue (n = 112) in BMPR1ΔK-injected animals showed the greatest degree of asymmetry (Fig. 5), with 39% of animals showing a reduction or loss of the left foregut (Fig. 3D', arrow denotes the right foregut). 55% of animals show a wildtype, bipartite foregut (Fig. 3B'). Only 6% of animals showed a reduction or loss of the right foregut, and 55% showed a symmetrical foregut. In general, the foregut also appeared slightly smaller than that of uninjected control animals, but this was not quantified (Fig. 3A–D). Foregut asymmetry was the most consistent and striking phenotype showing a loss or reduction of left tissues after BMPR1ΔK-injection.

Ventral nerve cord

BMPR1ΔK-injected animals (n = 123) generally showed symmetrical left and right hemiganglia in the VNC (concentrations of nuclei on either side of the ventral midline; 89% Fig. 5), although many hemiganglia appeared farther apart from each other relative to controls (Fig. 3A–D). Very few animals lacked hemiganglia on either side (left-reduced: 5%; right-reduced: 3%). The connectives of the VNC ($5HT^+$, n = 22) were generally symmetrical (82%). Of the remaining injected animals, 14% had a loss of the right connectives, none had a loss of the left connectives and 4.5% were lacking connectives altogether (Fig. 3E–H). It is important to note that the first $5HT^+$ connectives originate from neurons on the opposite (contralateral) side of the brain (e.g. $5HT^+$ neurons in the right brain lobe send their axons along the left connectives in the VNC) [29]. *Ct-elav1*$^+$ tissue in the trunk (n = 29) was usually symmetrical (62%), yet a reduction of either side was common (left-reduced:10%; right-reduced: 7%). *Ct-elav1* expression was not measured but was generally weaker in BMPR1ΔK-injected animals relative to controls (Fig. 3I–L). Strikingly, even in animals with *Ct-elav1* expression in the brain, 21% had no *Ct-elav1* expression in the trunk. Overall, the VNC displayed the least asymmetry after BMPR1ΔK-injection.

Mesoderm

In the trunk, BMPR1ΔK-injected animals (n = 107) generally showed mesodermal bands on both sides (64%), but there was a strong asymmetry; 31% had a reduced or missing left mesodermal band, while only 1% showed a reduced or missing right mesodermal band (Figs. 3A–D, 5). This asymmetry corresponded directly to asymmetry in the ventral longitudinal muscle fibers in the trunk (n = 56); all animals with a reduced or missing left or right mesodermal band were also lacking the corresponding left or right ventrolateral longitudinal muscle. Of note, only the ventrolateral longitudinal muscles were consistently lost, while the lateral and dorsolateral longitudinal muscles were still intact. Circular muscle fibers were present but were fewer and less organized in regions of the trunk where the anterior-ventral longitudinal muscle was lacking (Fig. 3M–P). In the episphere, the muscle fibers around the brain were not scored because it was unclear whether their asymmetry was due to brain position or mesodermal disruption. Overall non-wildtype

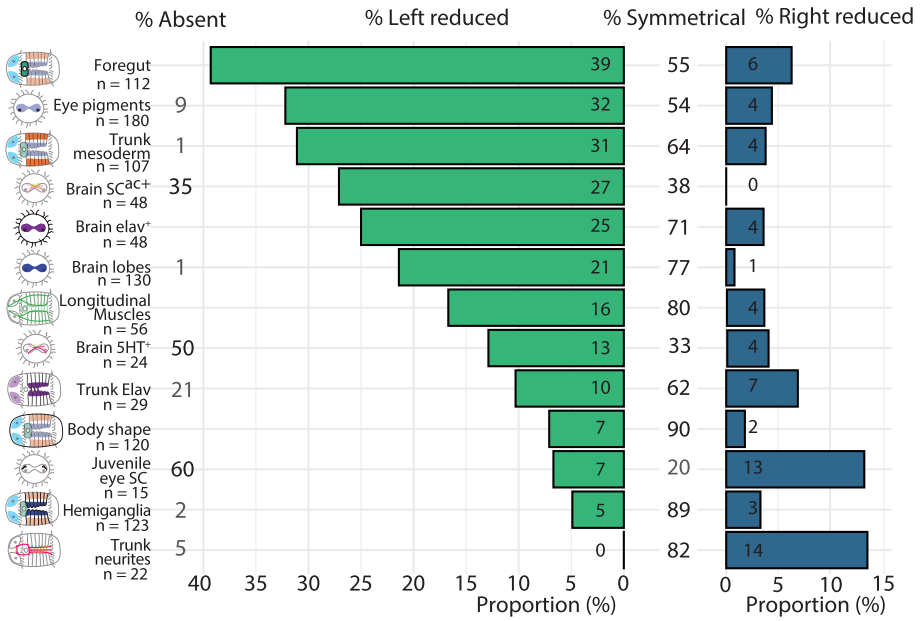

Fig. 5 Graphical representation of asymmetries in BMPR1ΔK-injected animals. Asymmetries are sorted from most to least proportion of animals with a reduction of the left side. Percentages are rounded to the nearest whole number

individuals showed a clear reduction in the left mesodermal bands that was reflected by a reduction in the left longitudinal muscles.

While most BMPR1ΔK-injected animals (n = 120) were generally straight along their anterior-posterior axis (90%), a small proportion showed a distinct bend in the trunk, mostly concave on the right side (7%) or left side (2%) of the trunk (Figs. 3D', L', 5). There was no correlation between body shape and which, if any, other asymmetries were present (e.g. some left and right bent animals lacked the left mesoderm, but not all), and no control animals showed a similar phenotype.

BMPR1ΔK interacts with BMP4 to change phenotypes

Previously, we reported that *C. teleta* larvae incubated in a 12h pulse of BMP4 protein starting at the 8-cell stage (1q) or just after the formation of the 4d micromere (~64-cell stage, 4q) displayed two different sets of phenotypes, both of which were symmetrical [11]. In contrast, when BMPR1ΔK-injected animals were incubated in BMP4 protein for 12h starting at 1q or 4q, they had strikingly different phenotypes than uninjected animals incubated in BMP4 for the same time window. Both 1q and 4q BMP-pulse, BMPR1ΔK-injected animals showed asymmetrical features, but in opposite directions (Fig. 6).

Eyes – larval pigment cells

As expected from previous work, uninjected, 1q BMP animals had zero larval eye pigment cells (n = 11) while only 38% of BMPR1ΔK-injected + 1q BMP animals (n = 31, Fig. 6) had zero larval eye pigment cells. The remainder mostly had 1 larval eye pigment cell (37%), although some had as many as 3 eye pigment cells (7%). Similarly, while uninjected, 4q BMP animals generally had the expected 3 larval eye pigment cells (n = 15, 87%), only 53% of BMPR1ΔK-injected + 4q BMP (n = 30) animals had 3 eye pigment cells, the remainder were mostly 2 or 4 eye pigment cells (20% each).

Asymmetries in the larval eye pigment cells were quite striking. As presented above, BMPR1ΔK-injected animals had about 30% left-reduced and 4% right reduced eye pigment cell. Surprisingly, BMPR1ΔK-injected + 1q BMP animals showed a strong loss of the right larval eye pigment cell (32%), with only 6% having a loss of left eye pigment cells. In contrast, BMPR1ΔK-injected + 4q BMP animals showed a strong reduction in left eye pigment cells (26%), with only a few animals lacking right eye pigment cells (9%). In summary, BMPR1ΔK-injected + 4q BMP animals were more similar to BMPR1ΔK-injected animals in lacking left larval eye pigment cells, while BMPR1ΔK-injected + 1q BMP animals were lacking the right larval eye pigment cell.

Foregut

1q BMP animals generally had a small, symmetrical foregut, similar to previously published results [11]. BMPR1ΔK-injected + 1q BMP animals (n = 31) also generally had a small foregut, but there was also a general

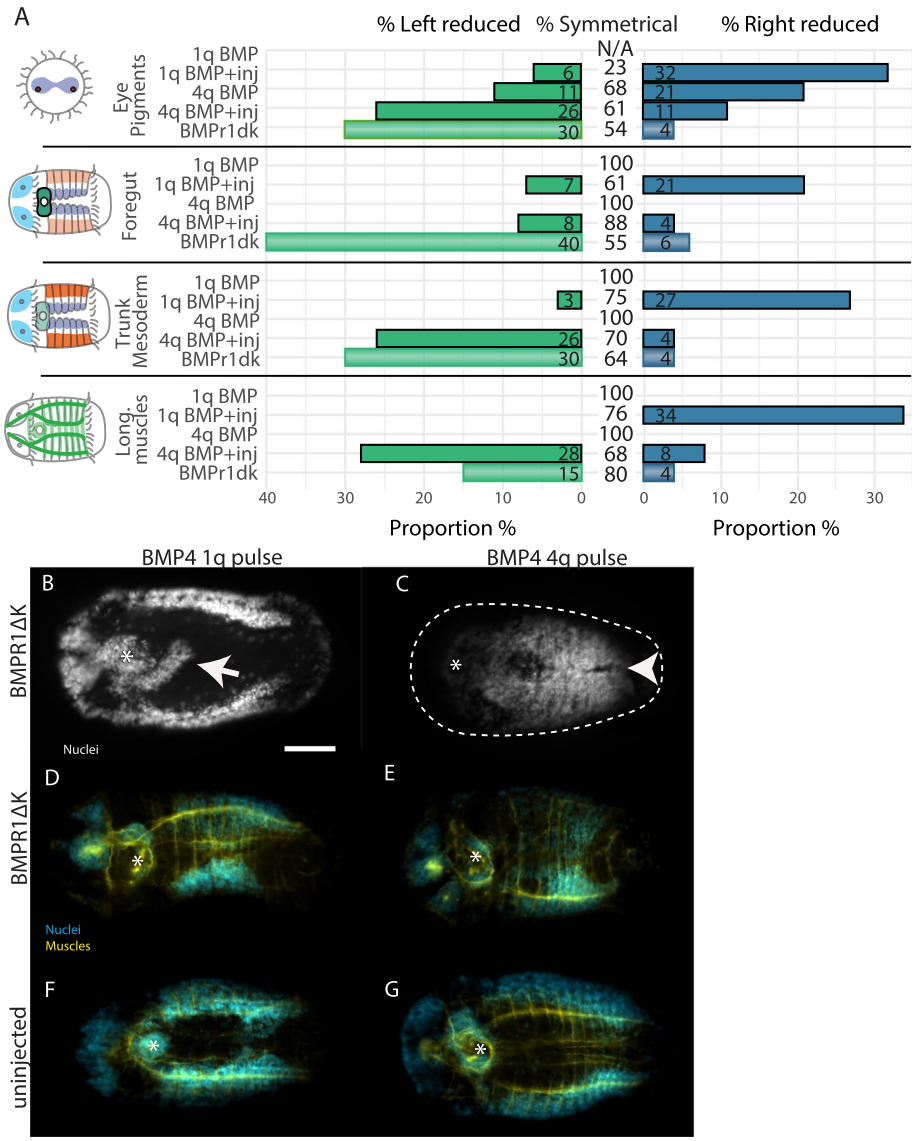

Fig. 6 BMPR1ΔK-injected phenotypes after a 12h pulse of BMP4 starting at 1q or 4q stage. **A** Graphical representation of asymmetries present in BMPR1ΔK-injected, BMP pulse animals. Percentages are rounded to the nearest whole number. **B**-**E** BMPR1ΔK-injected, ventral view. **F**-**G** uninjected, ventral view. **B**, **D**, **F** 1q BMP 12h pulse. **C**, **E**, **G** 4q BMP 12h pulse **B** BMPR1ΔK-injected + 1q BMP4 animal with elongated foregut (arrow). **C** BMPR1ΔK-injected + 4q BMP4 animal with merged hemiganglia (arrowhead). **D** BMPR1ΔK-injected + 1q BMP4 animal with reduced right foregut, mesoderm and trunk muscles. **E** BMPR1ΔK-injected + 4q BMP4 animal with reduced left mesoderm and trunk muscles. Nuclei: white or cyan; muscles: yellow; stomodeum: asterisk; scale bar: 50 µm

reduction of the right foregut (21%), with almost no loss of the left foregut (7%; Fig. 6). Additionally, 17% of animals showed a posterior elongation from the foregut that was not at all similar to the tripartite foregut seen in 4q BMP animals, but is similar to the right extension of the pharyngeal connection to the esophagus seen later in development [46] (Fig. 6B).

4q BMP animals generally have a tripartite foregut, similar to previously reported work [11]. In contrast, BMPR1ΔK-injected + 4q BMP animals (n = 30) did not show any foregut elongation or third lobe, and most had a wildtype foregut. Furthermore, there was no strong asymmetry in the foregut (8% loss of left, 4% loss of right foregut). Broadly speaking, both BMPR1ΔK-injected + 1q or 4q BMP animals were more similar to the BMP4 phenotype than the BMPR1ΔK-injected animals which generally had a reduction of the left foregut.

Trunk mesoderm

BMP4 pulses (1q or 4q) generally had no discernable effect on trunk mesoderm. BMPR1ΔK-injected + 1q BMP animals (n = 31) had a general reduction of the right trunk

mesoderm (27%), and right longitudinal trunk muscles (34%; Fig 7D) with almost no loss of the left mesoderm (3%) or muscles (0%; Fig. 6). In contrast, BMPR1ΔK-injected + 4q BMP animals ($n = 29$) had a general reduction of the left trunk mesoderm (26%; Fig 7E) and left longitudinal trunk muscles (28%) with almost no loss of the right mesoderm (4%) or muscles (7%). Broadly speaking, BMPR1ΔK-injected + 4q BMP animals were more similar to BMPR1ΔK-injected animals with a similar loss of the left mesoderm while BMPR1ΔK-injected + 1q BMP animals were lacking the right trunk mesoderm.

Neural tissue

We previously reported [11] that 1q BMP pulse animals showed a single central brain lobe, while 4q animals had 3 brain lobes: left, right, and midventral. There was no clear pattern in the number or position of brain lobes in BMPR1ΔK-injected + 1q or 4q BMP animals. Animals varied from 0–3 brain lobes in various positions. In the trunk, 25% of BMPR1ΔK-injected + 4q BMP animals ($n = 5/25$) had overlapping hemiganglia in the VNC. This phenotype was reminiscent of the ventral midline loss in animals treated with BMP after 4q [11] (Fig. 6C). In summary, there was too much variation in brain lobe number and location to find a clear pattern in BMPR1ΔK-injected, BMP-treated animals.

CRISPR knock-down of chordin-like causes right-biased asymmetry

As previously reported, the *C. teleta* genome lacks a homolog of Chordin but has one Chordin-like homolog, *Ct-chd-l*, which is expressed in cleavage-stage embryos and in the foregut, brain, and dorsal midline of developing larvae ([40], Webster et al. in prep). In other animals, Chordin-like (Chd-l) is a secreted BMP inhibitor, so we knocked down *Ct-chd-l* using CRISPR-Cas9 gene editing

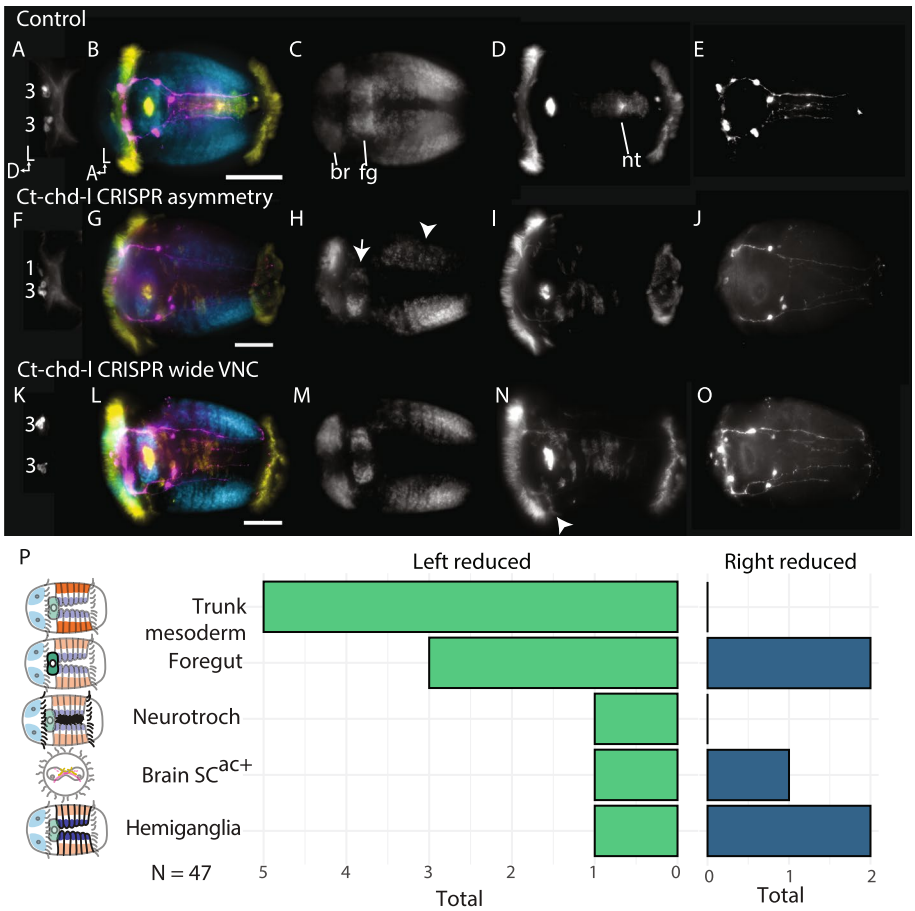

Fig. 7 *Ct-Chd-l* CRISPR phenotypes. **A**–**E** Control, uninjected animal. **F**–**J** Asymmetrical *Ct-Chd-l* CRISPR animals showing loss of left mesoderm (arrowhead) and reduced left foregut (arrow). Note: The apparent asymmetrical brain is an imaging artefact; **F** is a different animal than **G**–**J**. **K**–**O** *Ct-Chd-l* CRISPR animal with a wide VNC; arrowhead: separated prototroch. **P** Summary of asymmetrical phenotypes. **A**, **F**, **K** Anterior brain showing the number of SC^{ac+} cells. **B**, **G**, **L** merged images; **C**, **H**, **M** nuclei (cyan); **D**, **I**, **N** Acetylated tubulin (yellow); **E**, **J**, **O** Serotonin (magenta); Scale bars: 50 µm; A: anterior; D: dorsal; L, left lateral; br: brain; fg: foregut; nt: neurotroch

to disrupt BMP signaling. Of animals co-injected with Cas9 protein and two gRNAs targeting *Ct-chd-l* (Fig. 7), 21% (10/47) appeared wild-type, and 20% (9/47) failed to gastrulate. Strikingly, a few (9%) lacked the VNC and neurotroch altogether. 22% (10/47) of injected animals had a clear asymmetrical phenotype, with features that were weaker on one side compared to the other, as well as a wide, disorganised ventral midline (Fig. 7F–J); 6 had weaker left features, including lack of the left trunk mesoderm (5), a smaller left foregut (3), reduced left hemiganglia (1), fewer left SC^{ac+} cells (Fig. 7F; 2), and fewer left neurotroch cilia (1). Three asymmetrical animals showed weaker right features including a smaller right foregut (2), reduced right hemiganglia (2), fewer right SC^{ac+} cells (1), and fewer right neurotroch cilia (1). Most larvae (30%) showed a relatively normal head and small disruptions to the VNC: the VNC connectives were further apart and there were fewer cells in the wider neurotroch (Fig. 7K–O; 14/47). Some injected animals (8) showed a separation in the prototroch, where a few ciliated cells posterior to the prototroch (Fig. 7N arrowhead). This may indicate that secondary prototroch cells were displaced posteriorly. In summary *Ct-chd-l* CRISPR showed a similar reduction in left trunk mesoderm and foregut compared to BMPR1ΔK-injected animals, but showed very little evidence of affecting the brain.

Discussion

To date, there are only a few papers published that have tested the function of signaling receptors in spiralians; our results add to this work and provide two conclusions that transcend spiralian development. Firstly, we further demonstrate that BMP signaling does not block neural specification or control D-V axis formation in the annelid *C. teleta.* This, along with data from other annelids and spiralians, suggests that a conserved function for BMP signaling is not maintained across Bilateria. Secondly, we report an asymmetrical loss of left tissues in response to a dominant-negative Ct-BMBPR1 construct in *C. teleta*, a phenotype for which we could not find a precedent in the literature.

BMPR1ΔK::mVenus does not increase neural tissue

In vertebrates and insects, opposing gradients of BMPs and their secreted antagonists (e.g., Chordin) generate a gradient of BMP signaling that establishes tissues along the D-V axis. The neuroectoderm is specified in areas with no BMP signaling (e.g., high levels of antagonists), dorsal in vertebrates and ventral in arthropods. If the function of BMP signaling in establishing the neuroectoderm is conserved in annelids, we would predict that blocking function of Ct-BMPR1 should expand the domain of neuroectoderm and disrupt or abrogate D-V axis formation (e.g., ventralize animals). In *Xenopus laevis*, a dominant-negative BMP receptor caused a second body axis ventrally [34] and increased neural tissue in animal cap explants [47]. In *Drosophila melanogaster,* injection of dominant-negative forms of BMPR1 orthologs SAX and TKV each caused ventralization of the embryo (loss of the dorsal aminoserosa) [48]. We did not observe similar phenotypes in *C. teleta*. Elongated animals showed a relatively normal D-V axis in the trunk, where the expression of *Ct-elav1* in the VNC was generally symmetrically reduced in BMPR1ΔK-injected animals relative to controls. In addition, $5HT^{+}$ and ac-Tub^{+} cells and neurites were reduced asymmetrically in both the head and trunk of BMPR1ΔK-injected animals. In the brain, neural tissue originating from the right side generally resembled the wild-type condition without evidence of increased neural tissue. Overall, expression of BMPR1ΔK may have decreased neural tissue in the trunk, rather than increasing it. Our data further support the hypothesis that BMP signaling is not required for neural delimitation in *C. teleta* and likely more broadly in Spiralia [10, 11, 17].

BMPR1ΔK::mVenus may affect spiralian blastomere quadrant identity

Spiral cleavage is an important aspect of spiralian development, where cell fates can be traced from the earliest cleavages, creating four quadrants, A, B, C and D. In some spiralians, blastomeres in the D quadrant contribute to dorsal tissues while blastomeres in the B quadrant contribute to ventral tissues. Furthermore, in several spiralians, one or more D-quadrant blastomeres act as the D-V organizer by conditionally specifying fates [49]. This has led to the hypothesis that early during spiral cleavage, the D-to-B axis represents the D-V axis in different larval forms and in adults that develop by gradual metamorphosis. In contrast, the A-to-C axis represents right-left axis after gastrulation [49, 50]. However there is a great deal of unexplored variation in spiralian development [49]. Neither *C. teleta* nor *P. dumerilii* follow the D-to-B correlation with the D-V axis [51]. For example, in *C. teleta* the left and right trunk mesodermal bands are formed by C- and D-quadrant cells, respectively [41]. Fate maps and blastomere isolation studies in spiralians have highlighted how cell fate specification occurs very early in development and can be autonomous, although fates can be labile [52–57]. Our previous work suggested that BMP signaling may play a role in establishing quadrant identity during cleavage [11]. Specifically, we hypothesized that high levels of BMP signaling (e.g. ectopic BMP) during cleavage shifts blastomeres closer to D-quadrant fates rather than B-quadrant fates. Our data here are less clear. The tissues affected by BMPR1ΔK included tissues

mostly from the A-quadrant and D-quadrants: left eye (derived from 1a), left-ventral brain (minor contribution from 1a) and left foregut (2a), left-dorsal brain (1d) and left trunk mesoderm (3d). For the A-quadrant, we did not look for an effect of BMPR1ΔK on 3a (head mesoderm) because the episphere was too disorganized, or 4a (endoderm). For the D-quadrant, we did not expect an effect on 2d because it is hypothesized to be specified autonomously and is the organizer, and we did not score an effect on 4d since it makes too few tissues to easily recognize a disruption. Micromeres 1b, 1c, 2c, and 3c did not seem affected by BMPR1ΔK, and other micromere fates were not scorable.

If we assume that BMPR1ΔK causes quadrant fate changes opposite to those caused by ectopic BMP, we would expect a change from D- to A/C- to B-quadrant fates. We see this for A-quadrant tissue. The lack of left eye and left foregut tissue could be interpreted as a B-quadrant fate. We would also expect D-quadrant tissue to show a C-, B-, or A-like fate. It could be argued that the D-quadrant tissue also shows a B fate, with a lack or reduction of brain tissue and trunk mesoderm. In contrast, we should also expect the C-quadrant to move towards a B-like fate, which we did not find. Instead, the C-quadrant cells appeared to largely produce wild-type tissues with an intact right brain, eye, mesoderm, and foregut. This could indicate that the C-quadrant cells have a separate/redundant, possibly autonomous, mechanism for specification that does not involve BMP signaling. Given these results, we hypothesize that BMPR1ΔK affects some of the signals important for quadrant identity, which could explain why A- and D-quadrant cells may be switching to a B-quadrant fate, whereas C-quadrant cells remain relatively unaffected.

Interestingly, the asymmetrical phenotype was not the most common phenotype in BMPR1ΔK-injected animals. The majority of all BMPR1ΔK-injected animals failed to develop properly, producing a broad range of unelongated embryos that were difficult to categorize beyond the presence of an anterior-posterior axis. These embryos were more common in higher mRNA injection concentrations and appeared to have a catastrophic disruption of development. The asymmetrical phenotypes seen in most elongated, BMPR1ΔK-injected animals may represent only a mild disruption of BMP signaling resulting from heterogeneity either in terms of concentration, timing, or mosaicism of BMPR1ΔK. Interestingly, adding ectopic BMP did increase the proportion of animals that elongated and more so with a later BMP addition, suggesting some degree of phenotypic rescue (BMPR1ΔK-injected animals: 44% ± 5.3 SE elongation; 1q BMP4 + BMPR1ΔK: 76% elongation, 4q BMP4 + BMPR1ΔK: 88% elongation; 1 brood). Unfortunately, we cannot be more precise because levels of mVenus fluorescence did not correlate with severity of larval phenotypes. The unelongated embryos could represent highly affected animals in which all tissues changed to a B-quadrant fate, leaving little recognizable tissue or axes. It is important to note that B-quadrant cells do not generate "ventral" fates in *C. teleta*, and a shift towards B-quadrant identities would not be a ventralization of the animals.

Given this potential function of BMP signaling in spiralian blastomere quadrant identity, it is possible that D-V axis specification and possibly neural specification was ancestral for bilaterians, but the molecular mechanisms controlling these processes have since diverged significantly in spiralians, especially in Pleistoannelida. In this scenario, somewhere along the evolution of spiralians, the ancestral gene regulatory network for D-V axis formation (i.e., a BMP signaling gradient combined with activation of the MAPK cascade) shifted to be used for quadrant identity. For example, we previously published that the 5' end of SMAD1/5/8 mRNA in *C. teleta* is truncated and lacks the nuclear localization signal, something not seen in other spiralians [11]. Furthermore, in *C. teleta* Activin/Nodal is required for dorsal-ventral (D-V) axis formation [8] rather than BMP as in leeches [20] and molluscs [17, 18]. Along this evolutionary trajectory, molecular specification of CNS fate either diverged so much as to be unrecognizable or came under control of a separate GRN.

Understanding the molecular effect of BMPR1ΔK::mVenus has a number of confounding factors

The timing of events is critical during development. We showed this previously in the case of BMP signaling in *C. teleta* embryos, where early cleavages occur approximately every hour [11]. The timing of ectopic BMP dramatically changed the resulting phenotype; adding BMP prior to 4q caused a loss of eyes and a radialized brain, while adding BMP even an hour later, after the birth of 4d, instead caused a third eye and brain lobe to form. Although we demonstrated that *BMPR1ΔK::mVenus* is expressed in injected zygotes, the exact timing of BMPR1ΔK activity could not be determined and may be variable. mVenus fluorescence appeared within a few hours of injection and sometimes lasted for days, and injected embryos without observable mVenus expression showed the same phenotype as animals with mVenus fluorescence. This is not surprising because dominant-negative mutations can have a strong effect on signaling pathways, even in small concentrations [58]. This uncertainty makes it difficult to hypothesize about the mechanism behind the phenotypes caused by

BMPR1ΔK::mVenus since we lack data about the timing of BMPR1ΔK::mVenus activity.

Further difficulties in how to interpret our results arise from the fact that almost nothing is known about the BMP signaling pathway in spiralians, so we must make assumptions based on the data available from other animals. However, even in well-studied groups, the physical interactions between TGF-β family signaling pathways are still being elucidated, making comparisons difficult. For example, Tajer et al. [59] demonstrated that in mice, D-V axis formation requires both BMPR1 and ACVR1, which contradicts our previous understanding of vertebrate D-V axis organization. Not all BMP signaling passes through BMPR1 (ALK3/6), and SMAD1/5/8 is not exclusively phosphorylated by BMPR1. For example, in human myeloma and liver carcinoma cells, Olsen et al [60] showed that ectopic Activin can phosphorylate SMAD1/5/8 via ALK2 (ActivinR1), and knockdown of the type II receptor BMPR2 increases pSMAD1/5/8 via BMP6, BMP7, and BMP9 and ALK2. BMP7 can also phosphorylate SMAD1/5/8 via ALK2 [61]. Furthermore, BMPR1ΔK may reduce the availability of BMPR2 receptors in the system due to its effect as a dominant negative in hippocampal progenitor cells [62]. Our data suggests that not all of our assumptions about BMP signaling in spiralians are true, and further targeted study is required.

BMPR1ΔK::mVenus acts early during cleavage

We compared the phenotypes between BMPR1ΔK-injected animals with early ectopic BMP (12h pulse at 1q) to animals with a later ectopic BMP pulse (12h pulse at 4q). In general, the 4q BMP pulse had little effect on the BMPR1ΔK phenotype, whereas there was a clear difference in the phenotype of the BMPR1ΔK-injected + 1q BMP animals when compared to only BMPR1ΔK-injected animals. Specifically, an early (1q) BMP pulse reversed the phenotypes, producing a general loss of right tissues instead of left tissues. This fits well with the effects of just a BMP pulse, where the effects of a 1q pulse were dominant to a 4q BMP pulse [11] We predict that BMPR1ΔK irreversibly altered fates prior to 4q, otherwise the 4q BMP pulse should have changed the BMPR1ΔK phenotype. A full understanding of the interaction between BMPR1ΔK and BMP requires understanding the timing of BMPR1ΔK activity relative to when specific blastomeres are born. The earliest time we predict that BMPR1ΔK protein is active is around 5 h after injection of the mRNA, or ~32-cell (3q) stage, when we first see mVenus fluorescence, although there could have been variation depending on injection timing (± 1 h prior to first cleavage). Thus, BMPR1ΔK activity could begin acting before the 4q BMP pulse, but not likely before the 1q BMP pulse. More data will be required to tease apart the complex interactions between developmental timing and the relative timing of BMPR1ΔK and BMP4 activity.

BMPR1ΔK::mVenus may play a role in left-right axis formation

Our strongest evidence to support the idea that BMPR1ΔK affects left-right specification, whether through quadrant specification or otherwise, comes from the symmetry-reversing effect of BMPR1ΔK injection with an early BMP pulse. BMPR1ΔK generally caused a loss of left tissues, whereas adding BMP at 1q caused a general loss of right tissues instead.

In other animals, including some spiralians, Nodal and Pitx break symmetry along the left-right axis and disrupting Nodal signaling results in mirror-image symmetry. Nodal is expressed asymmetrically in molluscs [63] and brachiopods [64]. Knocking down Nodal signaling in the gastropod *Biomphalaria glabrata* with the drug SB-431542 often disrupted gastrulation, but the other major phenotype was uncoiled shells [63]. Adding recombinant Activin also has an asymmetrical effect in the snail *Crepidula fornicata* [65]. Overexpression resulted in abnormally symmetrical shells and a loss of torsion, presumedly by interfering with endogenous Nodal signaling. These phenotypes, which represent a loss of asymmetry, are in contrast to our reported asymmetrical loss of normally symmetrical tissues. We could not find any other reports of asymmetrical tissue loss due to manipulating signaling pathways for comparison. The closest analog we found is the loss of autonomously-specified tissues after blastomere isolation or ablation, where the cells fated to develop into a specific tissue are removed [52, 56, 66]. For example, in *X. laevis*, while a single blastomere from the two-cell stage will normally form an entire embryo, in the absence of wound healing, that same blastomere will only form a left or right half of an embryo [67].

Preliminary testing of the function of Nodal signaling during *C. teleta* development found no phenotypic effect of adding a wide range of concentrations (250, 500 and 1000 ng/mL) of recombinant human Nodal protein (R&D Systems 3218-ND) to embryos at different times (data not shown). In addition, ectopic Nodal protein did not affect pSMAD2/3 (D27F4, Cell Signaling) or pSMAD1/5/8 levels during cleavage or gastrulation stages, and ectopic BMP4 protein did not affect nuclear pSMAD2/3 levels (data not shown). It is possible that human recombinant Nodal does not interact with the Nodal signaling pathway in *C. teleta*.

Chd-l CRISPR affects the trunk and can produce asymmetries

Chordin/Sog is a critical extracellular antagonist of BMP signaling. While many annelids appear to have lost *chordin* from their genomes, they do have a related gene, *chordin-like* [27], which is thought to act in a similar manner. In zebrafish, Chordin and Chordin-like homologs have at least partially redundant function in regulating D-V axis formation [68], *Chd-l* transcripts from *Hydra vulgaris* can prevent BMP signaling in zebrafish [69], reinforcing the idea that Chd-l is also a BMP agonist. *Ct-Chd-l* is expressed throughout larval development, starting as early as 1q (8-cell stage [11]). As a result, we predicted that knocking out *Ct-chd-l* with CRISPR should have a similar effect to adding ectopic BMP; both should increase the effective availability of BMP in the embryo. This was not wholly the case. While ectopic BMP had little effect on trunk morphology except for a loss of the ventral midline and either loss or ectopic formation of foregut tissue, *Ct-chd-l* CRISPR almost entirely affected the trunk, even reducing trunk formation altogether in 9% of cases. *Ct-chd-l* CRISPR also mirrored BMPR1ΔK by producing asymmetrical effects. 20% of *Ct-chd-l* Cas9-injected animals had similar asymmetrical phenotypes to those found in BMPR1ΔK-injected animals. Unlike BMPR1ΔK-injected animals, phenotypes in the episphere were less common than trunk phenotypes, and there was a lower proportion of animals with a reduction of left tissues.

Trying to decipher how these results inform our understanding of BMP signaling is complicated. We did not examine intermediate developmental stages, so we cannot separate early and late effects of *Ct-Chd-l.* Furthermore, there may be maternal *Ct-chd-l* present that could play a critical role early in development and would not be affected by CRISPR. Lastly, not only are the functional differences between Chordin and Chordin-like unclear, but Chordin does not only act as a BMP agonist but can also act as a transporter. In *D. melanogaster* and *Tribolium castaneum*, Chordin/Sog binds BMP/DPP and transports it along a diffusion gradient [70], a mechanism that may also affect spiralian development, especially after gastrulation. Overall, our *Ct-chd-l* CRISPR results complement the BMPR1ΔK results, especially by producing a similar asymmetrical pattern and by having minimal effects on D-V axis and neural tissue.

Conclusions

Here we have demonstrated the first injected functional mRNA construct in *C. teleta* and identified further questions regarding the function of BMP signaling, specifically related to left-right symmetry. As previously reported, disrupting BMP signaling did not disrupt neural specification. Instead, we think that BMP plays a role in specifying quadrant identity. Specifically, we showed that introducing the kinase-deficient BMPR1ΔK caused a persistent left-reduced phenotype where the left eye, brain lobe, foregut, and mesoderm are reduced or lost, and adding early ectopic BMP4 reversed this phenotype, leading to a similar loss or reduction of right tissues. In addition, we showed that knocking down *Ct-chd-l* with CRISPR/Cas9 gene editing also produced an asymmetrical phenotype with a loss of left tissues, but this phenotype was present in the trunk rather than in the episphere. We believe this is a fascinating system to further elucidate the key role that BMPs play in the context of spiral cleavage, and in particular how the rigid framework of spiral cleavage is fundamentally different and can lead to key insights into the general rules of developmental genetics.

Abbreviations

1q	first-quartet (8-cell stage)
4q	fourth-quartet (~64-cell stage)
aa	amino acid
Alk	Activin Receptor-like Kinase
BMP	Bone Morphogenetic Protein
BMPR1	BMP Receptor 1
BMPR2	BMP Receptor 2
CNS	central nervous system
Chd/Sog	Chordin/Short Gastrulation
Chd-l	Chordin-like
D-V	dorsal-ventral
GRN	gene regulatory network
SMAD	Suppressor of Mothers against Decapentaplegic
stage	st.
TGF-β	Transforming Growth Factor β
VNC	ventral nerve cord

Supplementary Information

The online version contains supplementary material available at https://doi.org/10.1186/s13064-024-00181-7.

Supplementary Material 1.

Supplementary Material 2.

Supplementary Material 3.

Acknowledgements

The authors thank R. Bellin at the College of the Holy Cross for access to their confocal microscope. We would also like to thank José (Chema) Martín-Durán and an anonymous reviewer for their helpful comments.

Authors' contributions

The authors confirm contribution to the paper as follows: study conception and design: NBW and NPM; data collection: NBW; analysis and interpretation of results: NBW and NPM; draft manuscript preparation: NBW and NPM. All authors reviewed the results and approved the final version of the manuscript.

Funding

This work was supported by the National Science Foundation [Continuing grant #1656378].

Availability of data and materials
The datasets used and/or analyzed during the current study are available from the corresponding author on reasonable request.

Declarations

Ethics approval and consent to participate
Not applicable.

Consent for publication
Not applicable.

Competing interests
The authors declare no competing interests.

Author details
[1]Biology Department, Clark University, 950 Main Street, Worcester, MA 01610, USA. [2]Biology Department, University of Saskatchewan, 112 Science Place, Saskatoon, SK S7N 5C8, Canada.

Received: 18 September 2023 Accepted: 20 March 2024
Published online: 02 May 2024

References

1. Mieko Mizutani C, Bier E. EvoD/Vo: the origins of BMP signalling in the neuroectoderm. Nat Rev Genet. 2008;9(9):663–77.
2. Bond AM, Bhalala OG, Kessler JA. The dynamic role of bone morphogenetic proteins in neural stem cell fate and maturation. Dev Neurobiol. 2012;72(7):1068–84.
3. Gámez B, Rodriguez-Carballo E, Ventura F. BMP signaling in telencephalic neural cell specification and maturation. Front Cell Neurosci. 2013;7. Cited 2018 May 22. Available from: http://journal.frontiersin.org/article/10.3389/fncel.2013.00087/abstract.
4. Genikhovich G, Fried P, Prünster MM, Schinko JB, Gilles AF, Fredman D, et al. Axis patterning by BMPs: cnidarian network reveals evolutionary constraints. Cell Rep. 2015;10(10):1646–54.
5. Arendt D, Nubler-Jung K. Comparison of early nerve cord development in insects and vertebrates. Development. 1999;126(11):2309–25.
6. De Robertis EM. Evo-devo: variations on ancestral themes. Cell. 2008;132(2):185–95.
7. Denes AS, Jékely G, Steinmetz PRH, Raible F, Snyman H, Prud'homme B, et al. Molecular Architecture of Annelid Nerve Cord Supports Common Origin of Nervous System Centralization in Bilateria. Cell. 2007;129(2):277–88.
8. Lanza AR, Seaver EC. Functional evidence that Activin/Nodal signaling is required for establishing the dorsal-ventral axis in the annelid *Capitella teleta*. Development. 2020 Sep 15;147(18):dev189373.
9. Lanza AR, Seaver EC. An organizing role for the TGF-β signaling pathway in axes formation of the annelid *Capitella teleta*. Dev Biol. 2018;11(435):26–40.
10. Martín-Durán JM, Pang K, Børve A, Lê HS, Furu A, Cannon JT, et al. Convergent evolution of bilaterian nerve cords. Nature. 2018;553(7686):45–50.
11. Webster NB, Corbet M, Sur A, Meyer NP. Role of BMP signaling during early development of the annelid *Capitella teleta*. Dev Biol. 2021;1(478):183–204.
12. Martín-Durán JM, Hejnol A. A developmental perspective on the evolution of the nervous system. Dev Biol. 2021;1(475):181–92.
13. Lowe CJ, Terasaki M, Wu M, Jr RMF, Runft L, Kwan K, et al. Dorsoventral Patterning in Hemichordates: Insights into Early Chordate Evolution. PLOS Biol. 2006;4(9):e291.
14. Zhao D, Chen S, Liu X. Lateral neural borders as precursors of peripheral nervous systems: a comparative view across bilaterians. Dev Growth Differ. 2019;61(1):58–72.
15. Lyons DC, Perry KJ, Batzel G, Henry JQ. BMP signaling plays a role in anterior-neural/head development, but not organizer activity, in the gastropod *Crepidula fornicata*. Dev Biol. 2020;463(2):135–57.
16. Say T. Account of some of the marine shells of the United States. Acad Nat Sci Phil. 1822;2:124–55.
17. Lambert JD, Johnson AB, Hudson CN, Chan A. Dpp/BMP2-4 mediates signaling from the d-quadrant organizer in a spiralian embryo. Curr Biol. 2016;26(15):2003–10.
18. Tan S, Huan P, Liu B. Molluskan Dorsal-Ventral Patterning Relying on BMP2/4 and Chordin Provides Insights into Spiralian Development and Evolution. Mol Biol Evol. 2022;39(1):msab322.
19. Kuo DH, Shankland M, Weisblat DA. Regional differences in BMP-dependence of dorsoventral patterning in the leech *Helobdella*. Dev Biol. 2012;368(1):86–94.
20. Kuo DH, Weisblat DA. A new molecular logic for bmp-mediated dorsoventral patterning in the leech *Helobdella*. Curr Biol. 2011;21(15):1282–8.
21. Blake JA, Grassle JP, Eckelbarger KJ. Capitella teleta, a new species designation for the opportunistic and experimental *Capitella sp*. I, with a review of the literature for confirmed records. Zoosymposia. 2009;2:25–53.
22. Lanza AR, Seaver EC. Activin/Nodal signaling mediates dorsal–ventral axis formation before third quartet formation in embryos of the annelid Chaetopterus pergamentaceus. EvoDevo. 2020;11(1):17.
23. Carrillo-Baltodano AM. Understanding the evolution of animal body plans by looking at annelid neural development [PhD]. [Worcester, MA]: Clark University; 2019.
24. Martín-Durán JM, Passamaneck YJ, Martindale MQ, Hejnol A. The developmental basis for the recurrent evolution of deuterostomy and protostomy. Nat Ecol Evol. 2016;1(1):s41559-016-0005–16.
25. Molina MD, Neto A, Maeso I, Gómez-Skarmeta JL, Saló E, Cebrià F. Noggin and noggin-like genes control dorsoventral axis regeneration in planarians. Curr Biol. 2011;21(4):300–5.
26. Kenny NJ, Namigai EKO, Dearden PK, Hui JHL, Grande C, Shimeld SM. The Lophotrochozoan TGF-β signalling cassette - diversification and conservation in a key signalling pathway. Int J Dev Biol. 2014;58(6-7–8):533–49.
27. Martín-Zamora FM, Liang Y, Guynes K, Carrillo-Baltodano AM, Davies BE, Donnellan RD, et al. Annelid functional genomics reveal the origins of bilaterian life cycles. Nature. 2023;615(7950):105–10.
28. Grassle J, Grassle JF. Sibling species in the marine pollution indicator *Capitella* (polychaeta). Science. 1976;192(4239):567–9.
29. Meyer NP, Carrillo-Baltodano A, Moore RE, Seaver EC. Nervous system development in lecithotrophic larval and juvenile stages of the annelid *Capitella teleta*. Front Zool. 2015;11(12):27.
30. Seaver EC, Thamm K, Hill SD. Growth patterns during segmentation in the two polychaete annelids, *Capitella* sp. I and *Hydroides elegans*: comparisons at distinct life history stages. Evol Dev. 2005;7(4):312–26.
31. Altschul SF, Gish W, Miller W, Myers EW, Lipman DJ. Basic local alignment search tool. J Mol Biol. 1990;215(3):403–10.
32. Miura T, Tsukahara J, Hashimoto J. Lamellibrachia satsuma, a new species of vestimentiferan worms (Annelida: Pogonophora) from a shallow hydrothermal vent in Kagoshima Bay, Japan. Proceedings of the Biological Society of Washington. 1997;110(3):447–56.
33. Pyati UJ. Transgenic zebrafish reveal stage-specific roles for Bmp signaling in ventral and posterior mesoderm development. Development. 2005;132(10):2333–43.
34. Suzuki A, Thies RS, Yamaji N, Song JJ, Wozney JM, Murakami K, et al. A truncated bone morphogenetic protein receptor affects dorsal-ventral patterning in the early *Xenopus* embryo. Proc Natl Acad Sci. 1994;91(22):10255–9.
35. Roure A, Rothbächer U, Robin F, Kalmar E, Ferone G, Lamy C, et al. A multicassette gateway vector set for high throughput and comparative analyses in *Ciona* and vertebrate embryos. PLOS One. 2007;2(9):e916.
36. Layden MJ, Röttinger E, Wolenski FS, Gilmore TD, Martindale MQ. Microinjection of mRNA or morpholinos for reverse genetic analysis in the starlet sea anemone. Nematostella vectensis Nat Protoc. 2013;8(5):924–34.
37. Özpolat BD, Handberg-Thorsager M, Vervoort M, Balavoine G. Cell lineage and cell cycling analyses of the 4d micromere using live imaging in the marine annelid *Platynereis dumerilii*. Solnica-Krezel L, editor. eLife. 2017;6:e30463.
38. Neal S, de Jong DM, Seaver EC. CRISPR/CAS9 mutagenesis of a single r-opsin gene blocks phototaxis in a marine larva. Proc R Soc B Biol Sci. 2019;286(1904):20182491.
39. Concordet JP, Haeussler M. CRISPOR: intuitive guide selection for CRISPR/Cas9 genome editing experiments and screens. Nucleic Acids Res. 2018;46(W1):W242-5.

40. Joyce C. Evolution of Nervous System Centralization: Role of BMP Signaling in Neural Fate and Dorsal-Ventral Axis Specification in *Capitella teleta* [MSc.]. [Worcester, MA]: Clark University; 2017.
41. Meyer NP, Boyle MJ, Martindale MQ, Seaver EC. A comprehensive fate map by intracellular injection of identified blastomeres in the marine polychaete *Capitella teleta*. EvoDevo. 2010;1(1):8.
42. Eisig H. Die Segmentalorgane der Capitelliden. Mitt Zool Stat Neapel. 1878;1:93–118.
43. Gharbiah M, Cooley J, Leise EM, Nakamoto A, Rabinowitz JS, Lambert JD, et al. The Snail *Ilyanassa*: A Reemerging Model for Studies in Development. Cold Spring Harb Protoc.;2009(4):pdb.emo120-pdb.emo120.
44. Seaver EC, Paulson DA, Irvine SQ, Martindale MQ. The spatial and temporal expression of Ch-en, the engrailed gene in the polychaete *Chaetopterus*, does not support a role in body axis segmentation. Dev Biol. 2001;236(1):195–209.
45. Amiel AR, Henry JQ, Seaver EC. An organizing activity is required for head patterning and cell fate specification in the polychaete annelid *Capitella teleta*: New insights into cell–cell signaling in Lophotrochozoa. Dev Biol. 2013;379(1):107–22.
46. Boyle MJ, Seaver EC. Developmental expression of foxA and gata genes during gut formation in the polychaete annelid. Capitella sp I Evol Dev. 2008;10(1):89–105.
47. Xu RH, Kim JB, Taira M, Zhan SI, Sredni D, Kung HF. A dominant negative bone morphogenetic protein 4 receptor causes neuralization in xenopus ectoderm. Biochem Biophys Res Commun. 1995;212(1):212–9.
48. Neul JL, Ferguson EL. Spatially restricted activation of the SAX Receptor by SCW modulates DPP/TKV signaling in drosophila dorsal-ventral patterning. Cell. 1998;95(4):483–94.
49. Henry JQ. Spiralian model systems. Int J Dev Biol. 2014;58(6–8):389–401.
50. Grande C. Left-right asymmetries in spiralia. Integr Comp Biol. 2010;50(5):744–55.
51. Wilson EB. The cell-lineage of *Nereis*. A contribution to the cytogeny of the annelid body. J Morphol. 1892;6:361–480.
52. Carrillo-Baltodano AM, Meyer NP. Decoupling brain from nerve cord development in the annelid *Capitella teleta*: Insights into the evolution of nervous systems. Dev Biol. 2017;431(2):134–44.
53. Henry JQ, Lyons DC, Perry KJ, Chen CO. Establishment and activity of the D quadrant organizer in the marine gastropod *Crepidula fornicata*. Dev Biol. 2017;6(431):282–96.
54. Lyons DC, Perry KJ, Lesoway MP, Henry JQ. Cleavage pattern and fate map of the mesentoblast, 4d, in the gastropod *Crepidula*: a hallmark of spiralian development. EvoDevo. 2012;3(1):21.
55. Render J. Cell fate maps in the *Ilyanassa obsoleta* embryo beyond the third division. Dev Biol. 1997;189(2):301–10.
56. Sweet HC. Specification of first quartet micromeres in Ilyanassa involves inherited factors and position with respect to the inducing D macromere. Development. 1998;125(20):4033.
57. Wilson EB. Experimental studies on germinal localization. I. The germregions in the egg of *Dentalium*. J Exp Zool. 1904 May;1(1):1–72.
58. Veitia RA. Exploring the molecular etiology of dominant-negative mutations. Plant Cell. 2007;19(12):3843–51.
59. Tajer B, Dutko JA, Little SC, Mullins MC. BMP heterodimers signal via distinct type I receptor class functions. Proc Natl Acad Sci. 2021;118(15):e2017952118.
60. Olsen OE, Sankar M, Elsaadi S, Hella H, Buene G, Darvekar SR, et al. BMPR2 inhibits activin and BMP signaling via wild-type ALK2. J Cell Sci. 2018 ;131(jcs213512). Cited 2021 Apr 20.https://doi.org/10.1242/jcs.213512.
61. ten Dijke P, Yamashita H, Sampath TK, Reddi AH, Estevez M, Riddle DL, et al. Identification of type I receptors for osteogenic protein-1 and bone morphogenetic protein-4. J Biol Chem. 1994;269(25):16985–8.
62. Brederlau A, Faigle R, Elmi M, Zarebski A, Sjöberg S, Fujii M, et al. The bone morphogenetic protein type Ib receptor is a major mediator of glial differentiation and cell survival in adult hippocampal progenitor cell culture. Mol Biol Cell. 2004;15(8):3863–75.
63. Grande C, Patel NH. Nodal signalling is involved in left-right asymmetry in snails. Nature. 2009;457(7232):1007–11.
64. Martín-Durán JM, Vellutini BC, Hejnol A. Embryonic chirality and the evolution of spiralian left–right asymmetries. Philos Trans R Soc B Biol Sci. 2016;371(1710):20150411.
65. Truchado-García M, Perry KJ, Cavodeassi F, Kenny NJ, Henry JQ, Grande C. A small change with a twist ending - a single residue in EGF-CFC drives Bilaterian asymmetry. Mol Biol Evol. 2022;40(2):msac270.
66. Minokawa T, Yagi K, Makabe KW, Nishida H. Binary specification of nerve cord and notochord cell fates in ascidian embryos. Development. 2001;128(11):2007–17.
67. Kageura H, Yamana K. Pattern regulation in isolated halves and blastomeres of early *Xenopus laevis*. Development. 1983;74(1):221–34.
68. Branam AM, Hoffman GG, Pelegri F, Greenspan DS. Zebrafish *Chordin-like* and *Chordin* are functionally redundant in regulating patterning of the dorsoventral axis. Dev Biol. 2010;341(2):444–58.
69. Rentzsch F, Guder C, Vocke D, Hobmayer B, Holstein TW. An ancient chordin-like gene in organizer formation of *Hydra*. Proc Natl Acad Sci. 2007;104(9):3249–54.
70. van der Zee M, Stockhammer O, Levetzow C v., Fonseca RN d., Roth S. Sog/Chordin is required for ventral-to-dorsal Dpp/BMP transport and head formation in a short germ insect. Proc Natl Acad Sci. 2006;103(44):16307–12.

Publisher's Note